Biotechnology and Bioengineering

WILEY

BIOTECHNOLOGY AND BIOENGINEERING

ARTICLE

Impact of Adeno-Associated Virus Production on Capsid Heterogeneity and Product Quality

Alex Meola | Xiaotong Fu | Sarah Laughlin | Thomas Thiers | Luke Mustich | Eli Wiberg | Yongseok Kim | Qi Zhang | Eugenia Fandunyan | Richa Jaiswal | Matt Perez | Ben Rogers | Evan DaSilva | David Rouleau | Rudenc Lushi | Rob Horton | Brian Brazell | Michael Mercaldi | Jin Yin | James McGivney IV | Ify Iwuchukwu

Oxford Biomedica (US) LLC, Bedford, Massachusetts, USA

Correspondence: Xiaotong Fu (x.fu@oxb.com)

Received: 13 February 2026 | **Revised:** 16 April 2026 | **Accepted:** 20 April 2026

Funding: Oxford Biomedica (US) LLC

Keywords: AAV capsid heterogeneity | AAV product quality | anion exchange chromatography | deamidation | empty and full separation | production duration

ABSTRACT

Adeno-associated virus (AAV) capsids are inherently heterogeneous, arising from viral protein stoichiometric assembly, post-translational modifications, genome packaging, and manufacturing process conditions. Understanding how AAV manufacturing processes affect capsid heterogeneity and corresponding drug product quality impact is essential for AAV-based gene therapies. We investigated the effects of extended production duration and capsid localization at harvest on capsid heterogeneity. Analytical characterization revealed that prolonged production increased extracellular AAV concentrations but also elevated the proportion of empty capsids, overall hydrophobicity, and deamidation of viral protein (VP). These changes altered charge-dependent separation during anion exchange chromatography (AEX). Capsids derived from intracellular fractions showed even higher levels of deamidation and empty particles compared to extracellular populations, further impacting AEX purification performance. Collectively, these findings demonstrate that both production time and capsid localization significantly influence AAV purification process performance and critical quality attributes. Process control strategies to minimize capsid heterogeneity are consequently critical to ensure a consistent quality profile in AAV manufacturing.

1 | Introduction

Gene therapy has gained substantial momentum over the past decade due to its ability to deliver functional copies of genes for long-term, stable expression—offering the potential to treat a wide range of genetic disorders, particularly rare diseases. Among gene therapy vectors, adeno-associated virus (AAV) has emerged as a leading platform due to its favorable safety profile, low immunogenicity, and ability to mediate long-term gene expression in nondividing cells. AAV is a small, nonenveloped virus composed of 60 capsid subunits formed by 3 viral proteins (VPs), VP1, VP2, and VP3, with a single-stranded DNA genome encoding the gene of interest (GOI) (Bulcha et al. 2021; DiMattia et al. 2012). VP3, the most abundant and smallest protein, provides structural stability, while VP1 and VP2 play key roles in cellular entry and intracellular trafficking. During AAV production, VP proteins are expressed and assembled stochastically into capsids, yielding a heterogeneous population with variable VP stoichiometry. Genome packaging occurs after capsid assembly, producing a mixture of empty, partially filled, and fully packaged capsids (Wright 2014).

Although recent advances in AAV manufacturing have improved vector yield, purification efficiency, and control of process-related impurities (Ayuso et al. 2010; Clément and Grieger 2016; Dickerson et al. 2021; van Lieshout et al. 2023), certain product quality attributes, such as capsid heterogeneity, are not well understood. Capsid heterogeneity, defined as

variability in the physicochemical properties of AAV capsids, results from differences in VP composition, post-translational modifications (PTMs), genome packaging, and process conditions. These variations can influence vector purification, stability, and ultimately, therapeutic efficacy (Fuentes et al. n.d.; Giles et al. 2018; Wörner et al. 2021).

Recent advances in analytical techniques enabled more comprehensive characterization of capsid heterogeneity, allowing us to further investigate the root causes (Burnham et al. 2015; Fu et al. 2019; McColl-Carboni et al. 2024; Wu et al. 2025). In this study, we examined the impact of production duration and capsid localization (intracellular vs. extracellular) on AAV capsid heterogeneity. Specifically, we collected vectors harvested after 3 and 6 days of production, both located intracellularly and extracellularly, and analyzed productivity, genome packaging profiles, hydrophobicity, charge variants, and PTMs, particularly deamidation. Anion exchange chromatography (AEX) performance was also evaluated in the context of capsid heterogeneity. Finally, biological function was assessed via transgene expression, correlating capsid heterogeneity with product potency. These findings provide insight into the strategies of process optimization and quality control in AAV-based gene therapies to consistently produce high purity and efficacious viral vectors.

2 | Materials and Methods

2.1 | AAV Production and Harvest

HEK293 cells were transfected using a novel dual-plasmid platform. Transfected cultures were incubated in 2-liter bioreactors for either 3 or 6 days. As a control, detergent lysis was performed on Day 3 post-transfection, and the resulting whole-cell lysate was collected and processed through downstream purification. For the experimental arms, culture supernatants and cell pellets were separated by centrifugation on Days 3 and 6. Cell pellets were resuspended in fresh media, lysed using a detergent-based buffer, and purified independently from their corresponding supernatants.

2.2 | AAV Purification

The crude lysate was thawed overnight at ambient temperature and filtered with a 0.2 μm filter (Cytiva, MA, USA) before being loaded onto a POROS CaptureSelect AAV9 column (Thermo Fisher Scientific, MA, USA) connected to an ÄKTA Avant 25 (Cytiva, MA, USA). After re-equilibration and a series of washes, AAV product was eluted by lowering the pH. Eluate was collected into a container pre-aliquoted with pH neutralization buffer to bring the eluate to neutral pH. The neutralized affinity eluate was diluted with low-conductivity dilution buffer to adjust its pH and conductivity to enable AEX loading. An AEX column was used to separate empty and DNA-containing capsids via a step elution with an optimized conductivity. A fixed number of column volumes (CVs) of AEX eluate was directed to a container prefilled with neutralization buffer. Following the elution phase, an AEX strip was performed using a high-salt buffer to recover bound capsids via increased conductivity. The resulting strip fraction was immediately neutralized to minimize any potential impact on capsid properties and ensure stability. All samples were frozen at −80°C prior to analysis.

2.3 | Viral Genome Titer by ddPCR

VG titer was measured by standard droplet digital polymerase chain reaction (ddPCR). All test samples were treated with RNase-free DNase I and proteinase K prior to analysis. Processed samples were amplified in ddPCR Supermix (BioRad, CA, USA). Following the droplet generation via an oil:water emulsification, samples were amplified to the endpoint in a thermal cycler and subsequently scanned on a QX200 droplet reader (BioRad, CA, USA). Data were analyzed with QuantaSoft software (BioRad, CA, USA).

2.4 | Capsid Titer by Capsid ELISA

Capsid titer was determined by a commercially available ELISA kit (Progen, Heidelberg, Germany) specific to the AAV9 serotype and performed according to the manufacturer's instructions (Progen, Heidelberg, Germany).

2.5 | Packaging Determination by Analytical Ultracentrifugation

Quantification of percent full, partial, and empty AAV capsids was performed using an Optima AUC (Beckman Coulter). During the sedimentation process, scans were taken at 260 nm and compiled into SEDFIT. Analysis of AAV samples by the SEDFIT c(S) model yields a distribution of sedimentation coefficients with each peak in the distribution representing an intact AAV genome, product-related impurity in the form of partially packaged genome or residual nucleic acid impurities, or empty capsids. Integration of the individual peaks yields the sedimentation coefficient (S) and the relative concentration of each species in the distribution. A linear relationship between the S and the length (in nucleotides) of the packaged transgene can be used to predict the S value of a fully packaged AAV (Burnham et al. 2015).

2.6 | PTM Analysis by Liquid Chromatography–Mass Spectrometry (LC–MS)

PTMs were identified and calculated using recently published methods (Giles et al. 2018). Briefly, the samples were dried and denatured with 8 M guanidine-HCl (Fisher Scientific, PA, USA). In total, 10 mM dithiothreitol (Thermo Scientific, MA, USA) and 20 mM iodoacetamide (Thermo Scientific, MA, USA) were used for reduction and alkylation followed by 30 min of trypsin (Promega, WI, USA) digestion. The reaction was quenched with 1% formic acid. The Thermo Vanquish Flex UHPLC system (Thermo Fisher Scientific, Germany), coupled to a Thermo Q Exactive HF mass spectrometer (Thermo Fisher Scientific, Germany) with a data-dependent acquisition method, was utilized for data collection, and Skyline software (MacCoss Lab Software, Version 21.2.0.425) was used for PTM analysis (MacLean et al. 2010).

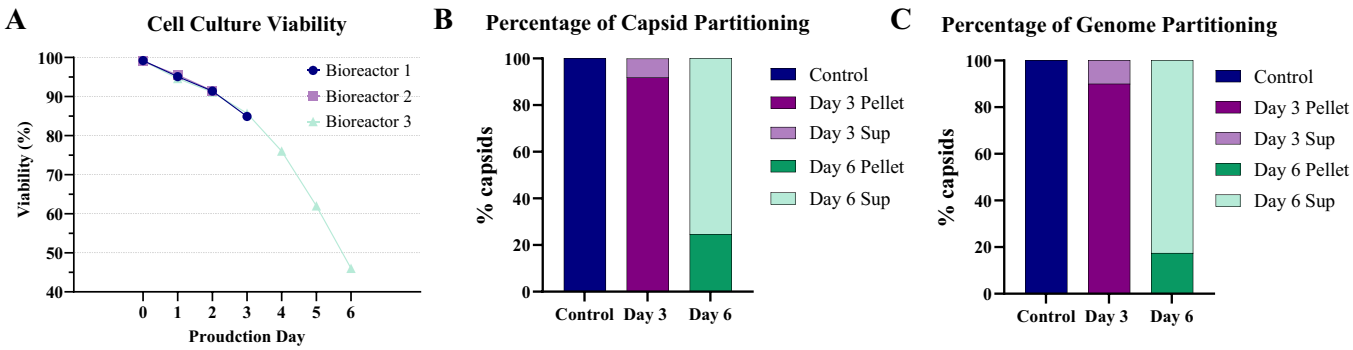

FIGURE 1 | AAV partitioning during upstream production. (A) Cell culture viability decreased in all bioreactors up to 6 days post-transfection. Day 0 is the day of transfection day. (B) The quantity of capsids detected in the harvested materials for the full-lysis control, Day 3 and Day 6 cell pellet and supernatant, respectively. At 3 days post-transfection, 8% of total capsid was detected in the supernatant, which increased to 82% at Day 6 post-transfection. (C) Genome titer was measured within the cell culture lysis control, Days 3 and 6 post-transfection. An identical trend to the capsid titer was observed for the genome titer measurement.

2.7 | VP Area and Purity Determination by Capillary Electrophoresis

VP purity and VP1:VP2:VP3 ratios were determined by capillary electrophoresis and performed in the presence of sodium dodecyl sulfate (CE-SDS). Samples, reference materials, and standards were heat-denatured in SDS-containing buffer and then separated at 18 kV on a PA800 Plus CE system with an uncoated, fused silica capillary (AB Sciex, MA, USA). As the proteins separate and pass through the capillary, analytes are detected spectrophotometrically by absorbance at 220 nm.

2.8 | Hydrophobicity Determination by HIC-HPLC

Hydrophobicity profiles were determined by high-performance liquid chromatography. Samples were diluted in an appropriate hydrophobic interaction chromatography (HIC) buffer. A volume of 40 µL for each sample was injected onto a TSKGel Butyl NPR (nonporous) 4.6 mm × 3.5 cm, 2.5 µm column (Tosoh Bioscience, PA, USA). A 6.4 column volume (CV) gradient was run from 0% to 100% elution buffer and an additional 5.2 CVs at 100% elution buffer were run to ensure all analytes eluted off the column prior to re-equilibration. Analytes were detected spectrophotometrically by fluorescence with absorbance at 280 nm and emission at 350 nm.

2.9 | In-Vitro Protein Expression

Expressed green fluorescent protein (GFP) was assessed by cellular imaging. HeLa RC32 cells (ATCC) were infected with test samples at a fixed MOI range. Following infection, cells were incubated at 37°C at 5% CO_2 for 48 h. The cells were then imaged by brightfield and fluorescence on a Celigo Image Cytometer (Nexelcom, MA, USA). Percent positive cell data were collected and log transformed, then plotted against MOI in PLA software (Stegmann Systems GmbH, Rodgau, Germany) to obtain a relative protein expression semi-log fit curve. The effective concentration at 50% activity (EC_{50}) from the reference was divided by the EC_{50} from the sample and multiplied by 100, yielding the percent relative protein expression (% RPE) result.

3 | Results and Discussion

3.1 | AAV Partitioning During Production

To evaluate how the production process affects capsid heterogeneity, AAV samples were characterized at different production time post-transfection. At 72 h post-transfection, AAV culture was spun down to generate cell pellet and supernatant samples. Cell pellets were resuspended in fresh media and lysed with detergent to release AAV for analysis, named as Day 3 Pellet, while the AAV in the supernatant was labeled as Day 3 Sup. Production time of 144 h was also investigated in the same approach, yielding samples as Day 6 Pellet and Day 6 Sup. A control sample, where full detergent lysis was conducted at 72 h without separating the cell pellet, was introduced as Control for comparison.

Cell culture viability was monitored during the production phase (Figure 1A). Post-transfection (Day 0), cell viability decreased to 85% on Day 3, and 46% on Day 6. An increase in capsids released was observed with increase in time spent in the bioreactor. This was verified by capsid ELISA results measured from the cell pellet between Days 3 and 6 (Figure 1B). At Day 3, 92% of AAV was detected in the cell pellet, with the capsid titer similar to the full-lysis control, while at Day 6, up to 75% of AAV capsids were detected in the supernatant. Genome titer measured followed the same distribution trend as capsid titer evaluation (Figure 1C). This result suggests that the majority of AAV collected from the standard Day 3 full lysis process are intracellular AAV. As cell viability drops, cell death leads to more AAV release extracellularly until cell lysis is performed. Interestingly, regardless of cell viability, the total concentration of capsids (pellet plus sup) remained consistent between Days 3 and 6, indicating that a minimum amount of AAV being produced post 72 h of transfection (Figure S1).

3.2 | Capsid Hydrophobicity Change During the Production Stage

Knowing that extended production time provides minimal benefit to overall AAV productivity, the impact of prolonged production on capsid heterogeneity was investigated. Hydrophobicity is a critical attribute indicating capsid physicochemical status, potentially altered by PTMs during AAV production. We purified AAV samples produced from each production condition and analyzed them using a HIC (HIC-HPLC) assay developed to assess capsid

hydrophobicity. Figure 2A displays retention time profiles for the control, Day 3 cell pellet, and Day 6 cell pellet samples. The AAV from the Day 3 cell pellet exhibited no detectable hydrophobicity change compared to the control sample, as 90% of the control sample's AAV population originated from the cell pellet (Figure 1B). However, an additional 3 days of production led to a modest increase in capsid hydrophobicity, indicated by the shift in retention time. A similar trend was observed when comparing supernatant samples collected on Days 3 and 6 (Figure 2B), where an increase in hydrophobicity was observed. We also noticed the Day 3 supernatant sample had a slightly lower retention time than the control, suggesting capsids in the supernatant are less hydrophobic compared to their intracellular counterparts. From a production duration perspective, given that the retention time shift was identical for the cell pellet and supernatant samples between 3 and 6 days, we concluded that the increase in hydrophobicity is attributable to the extended production duration regardless of AAV distribution within the culture.

This observed hydrophobicity shift is consistent with conformational changes known to occur during AAV intracellular trafficking. During the endosomal process, VP1u is externalized and exposes the hydrophobic phospholipase A2 (PLA2) domain, which is required for endosomal escape and nuclear entry. Prolonged residence in the production environment may promote similar structural transitions, thereby increasing capsid surface hydrophobicity (Kronenberg et al. 2005; Penzes et al. 2021; Popa-Wagner et al. 2012; Sonntag et al. 2006; Venkatakrishnan et al. 2013).

3.3 | AAV Packaging Differs Across Production Conditions

Given the significant impact of genome content on capsid heterogeneity, AAV packaging profile was evaluated under each production condition using analytical ultracentrifugation (AUC). The corresponding results are presented in Figure 3A,

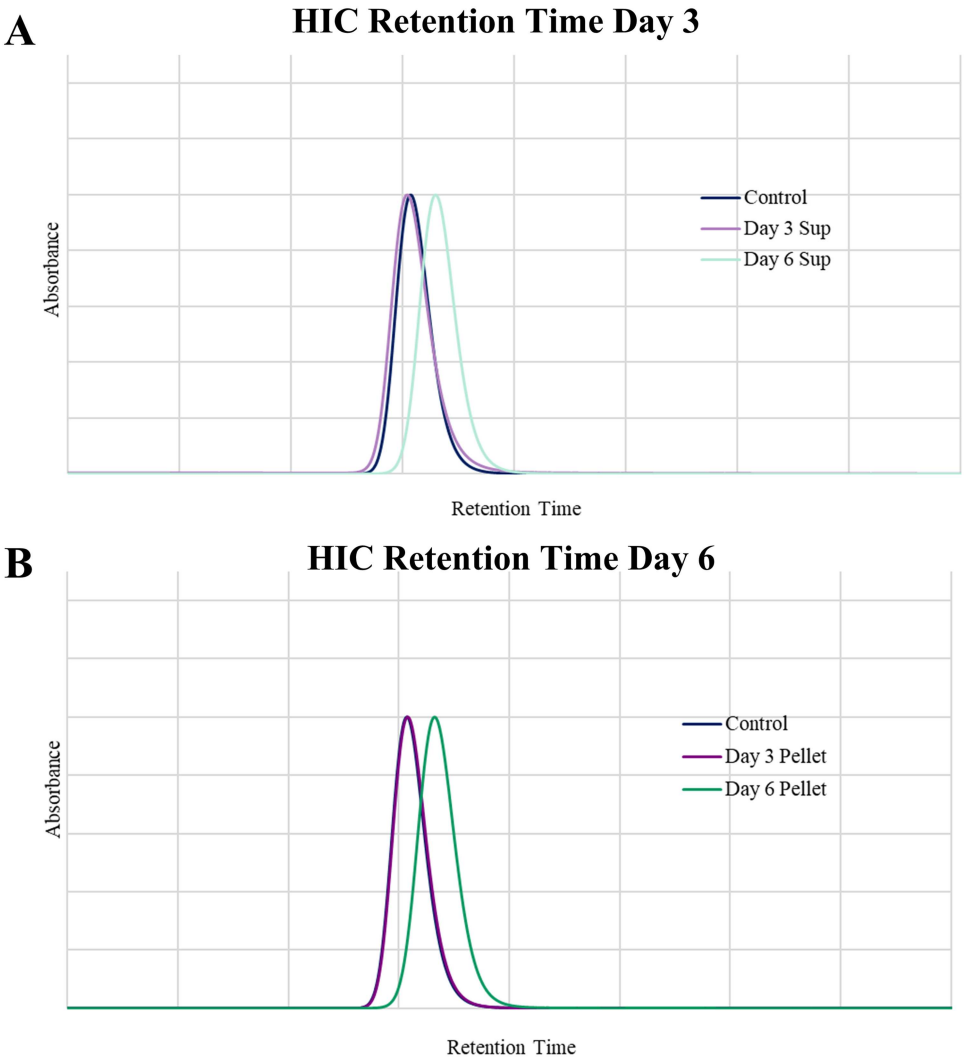

FIGURE 2 | Assess the hydrophobicity of affinity (AF) eluates from different production conditions using the HIC method. (A) HIC-HPLC chromatogram overlay of affinity eluates from Day 3 Full Lysis Control and Supernatant arms. Day 3 Supernatant had a slightly lower retention time than the control sample. A significant retention time shift was observed when production time was extended to 6 days. The increase in retention time suggests increased hydrophobicity of the tested samples, likely resulting from capsid surface modification. (B) HIC-HPLC chromatogram overlay of affinity eluates from Day 3 Full Lysis Control and the Pellet arms. Similar to the supernatant arms, the major retention time shift was caused by the extended production time.

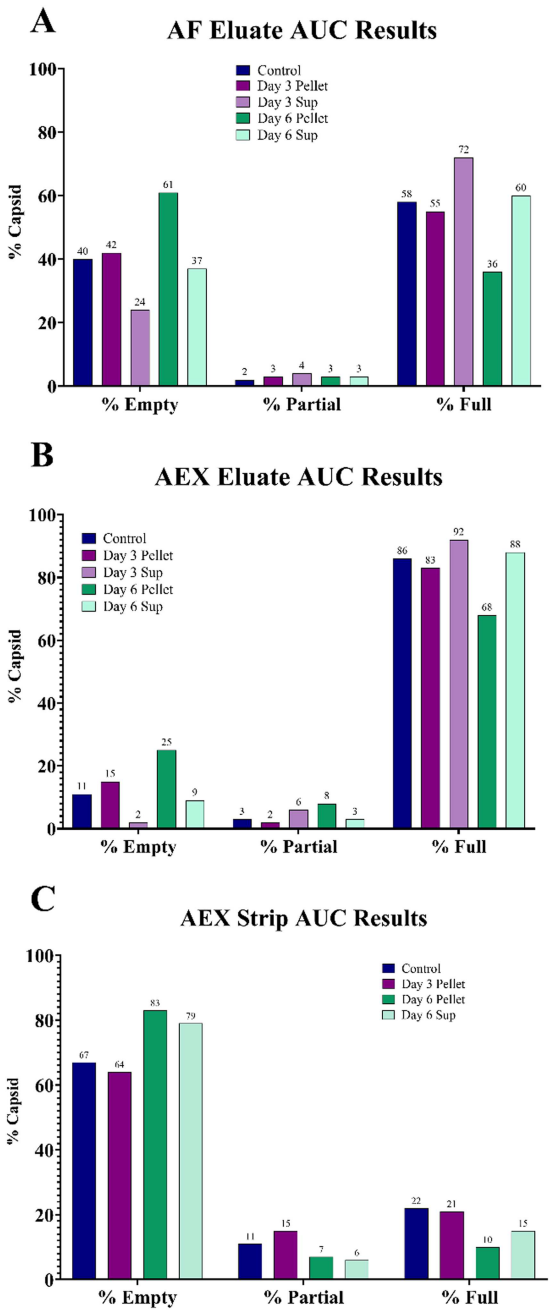

FIGURE 3 | Assess AAV subpopulations in the affinity eluate, AEX eluate, and AEX strip from each production condition using AUC. (A) AUC results of affinity eluate. Day 3 Pellet sample showed a similar %full as the full lysis control but decreased to 36% after 3 extra days. The supernatant sample started with higher %full at 72% and decreased to 60% between Days 3 and 6. (B) AUC analysis of the AEX eluate from each production condition. Most AEX eluates showed above 80% full capsids, indicating great empty and full capsid separation efficiency. The only exception was the Day 3 pellet sample, where the %full post-AEX purification was 68% due to extra empty capsids to start with. (C) AUC results of each AEX strip sample. The %full indicates that most capsids in the strip fraction are empty. Note that the AUC test of the AEX strip sample from Day 3 Supernatant was not valid due to low AAV concentration.

where AAV subpopulations are distinguished as "Full" (containing full-length GOI), "Partial" (containing truncated GOI), and "Empty" (lacking DNA content). To meet the purity and concentration requirements of the AUC method, samples were analyzed following affinity purification. Though neutralization was performed immediately to minimize impact on AAV capsid properties, the implementation of low pH elution during affinity chromatography may still alter the original stage of capsid. Therefore, all affinity purifications were kept consistent for each production condition to ensure accurate comparison.

Consistent with trends observed in AAV distribution and hydrophobicity, the Day 3 cell pellet exhibited a packaging profile comparable to the control condition (Figure 3A). In contrast, the extracellular AAV at Day 3 showed a markedly higher proportion of full capsids (%Full: 72%) relative to the cell pellet (%Full: 55%). By Day 6, the percentage of full capsids in the supernatant remained high (%Full: 60%) compared to the corresponding cell pellet (%Full: 36%). These findings suggest that the AUC profile changes are not solely a result of AAV release upon cell lysis. Rather, genome-containing AAV appears to be preferentially partitioned extracellularly at the beginning of production, as the %Full capsid of the Day 3 supernatant was 17% higher than the Day 3 pellet sample. However, as cell viability declined over time, increased cell death also contributed to the release of empty capsids, thereby reducing the overall %Full in the Day 6 supernatant. However, the specific biological mechanisms underlying this apparent selective partitioning were not explored further in this study. AUC sedimentation coefficient distribution plots were captured in Figure S2 for reference.

3.4 | VP Protein Stochastics During Production Stage

As discussed above, the stochastic assembly of VPs can contribute to AAV capsid heterogeneity. To evaluate the impact of production conditions on VP composition, purified AAV samples under each condition were analyzed by the capillary electrophoresis method (CE-SDS), with results summarized in Table 1. Affinity chromatography effectively removed most process-related impurities, resulting in product purity exceeding 99% across all tested conditions. Minor fluctuations in the relative abundance of VP1, VP2, and VP3 were observed under different production conditions, regardless of AAV localizations. However, these variations remained within the expected range of CE-SDS assay variability and did not show any statistically significant changes in VP ratios.

3.5 | VP1 Protein Deamidation During Production

PTMs of AAV capsid proteins, particularly deamidation events, have been implicated in capsid heterogeneity and altered vector functionality (Giles et al. 2023; Grieger et al. 2006). Of particular interest is the deamidation of asparagine residues within the VP1 region, which plays a critical role in AAV cell entry and intracellular trafficking. To assess the impact of production conditions on VP1 deamidation, we performed peptide mapping using LC–MS on each sample, focusing on the N57 residue, a known hotspot for deamidation. All samples were purified via affinity chromatography prior to LC–MS analysis to meet the purity requirement for analysis, which may have influenced the measured deamidation profiles relative to the native state

TABLE 1 | Assessment of purity via CE-SDS of each affinity product purified.

Arm	%purity	VP1%	VP2%	VP3%	VP ratios		
Control	99.7	8.3	9.6	81.9	1.0	1.1	9.9
Day 3 Pellet	100.0	8.3	9.2	82.5	1.0	1.1	10.0
Day 3 Sup	100.0	8.5	10.5	81.0	1.0	1.2	9.5
Day 6 Pellet	99.1	8.0	9.0	82.2	1.0	1.1	10.3
Day 6 Sup	100.0	7.9	9.3	82.8	1.0	1.2	10.5

during production. Nonetheless, as all purification conditions were identical for each sample, we believe the direct comparisons still provide a valid perspective for showing deamidation changes.

By Day 3 of production, deamidation of the N57 site in the cell pellet sample was tested as 36%, compared to 21% in the control and 10% in the supernatant (Figure 4B), indicating a drastically different rate of deamidation between intracellular and extracellular AAV. By Day 6, N57 deamidated substantially in both the cell pellet and supernatant fractions, measured as 20% and 11% increases, respectively. These findings not only support the hypothesis that prolonged production duration facilitates deamidation but also indicate the intracellular environment may accelerate deamidation. The reason for this observed trend was not further evaluated. The hypothesis is that intracellular AAVs are more prone to structural rearrangements or partial unfolding that expose the N57 site. One possible explanation is that capsids retained within cells are more likely to be empty, as supported by capsid content analysis (Figure 3A). The absence of a genomic payload may lead to reduced structural stability, which makes AAV more susceptible to chemical modifications such as deamidation over time (McColl-Carboni et al. 2024; Zhou and Wang 2023).

Additional modification sites, including N94, N452, and Q456, as well as phosphorylation and isomerization events, were also identified in this study. However, these modifications did not show statistical significance correlating to product quality measurements (Table S1).

3.6 | Capsid Heterogeneity Impacts AEX Chromatography

Capsid heterogeneity presents a significant challenge for AEX chromatographic enrichment of full capsid. Given that AEX separation is charge-based, heterogeneity in AAV charge profiles directly influences purification outcomes. After establishing that production duration can alter capsid heterogeneity, we conducted a linking study to examine its impact on AEX performance.

AUC was used to evaluate the capsid subpopulations captured in both the AEX eluate (desired product) and the AEX strip (impurities). Figure 3B displays the AUC profiles of AEX eluates from all production conditions. Under all conditions tested, the AEX process demonstrated effective %full enrichment. However, the final %full purity achieved was directly correlated to the initial packaging efficiency. For instance, the Day 3 supernatant, starting at 72% full, achieved 92% full post-AEX; in contrast, the Day 6 cell pellet, beginning at 36% full, reached only 68% full using the same AEX protocol. Further AUC analysis of AEX strip fractions (Figure 3C) showed that the strip peak was predominantly composed of empty capsids, with varying amounts of partial and full capsids. While AEX strip compositions were similar between Day 3 cell pellet and the Control samples, notable differences were observed over an extended production duration. At 3 days, AEX strip samples contained a higher proportion of full and partial capsids, whereas at 6 days, strip fractions had higher empty capsids (above 80%). These findings suggest that production duration not only impacts empty and full ratio of AAV samples, but it also alters the charge profiles of each AAV subpopulation, resulting in different AEX separation performance.

3.7 | N57 Deamidation Affects Charge-Based Separation

Although the AEX process demonstrated inherent robustness enriching full capsid, the observed charge profile variations led to additional characterizations of capsid heterogeneity post-AEX step. We hypothesized that N57 deamidation, as discussed above, contributes to the variability in AEX performance by altering capsid surface charge. To assess AAV charge variation, capsid binding behavior to AEX resin was used as a surrogate, with the proportion of capsids recovered in the AEX strip serving as an indicator of increased surface charge. Figure 4A is the correlation between the degree of N57 deamidation and the amount of capsid recovered in the AEX strip. A statistically significant correlation ($p = 0.02$, $R^2 = 0.87$) supports the hypothesis that deamidation at N57 leads to increased capsid negativity. To further confirm this finding, we compared deamidation levels in AEX eluates, AEX strips, and the corresponding affinity eluates from the same process stream (Figure 4B). Across five production conditions, LC–MS analysis showed reduced deamidation levels in the AEX eluates compared to their affinity-purified counterparts, while the AEX strip fractions were enriched in deamidated capsids, further supporting the association between deamidation and increase in negative charge.

To investigate any additional stoichiometric changes during the AEX process in addition to PTM, VP ratio and purity of AEX eluate and strip samples were measured by CE-SDS (Table 2A,B). No significant differences were observed in VP protein stoichiometry across samples, indicating that observed charge alterations were due to surface modifications (i.e., deamidation) rather than changes in capsid protein composition.

3.8 | Capsid Heterogeneity Affects AAV Functional Activity

To assess the impact of capsid heterogeneity on AAV functional activity, we measured the relative potency of AAV based on

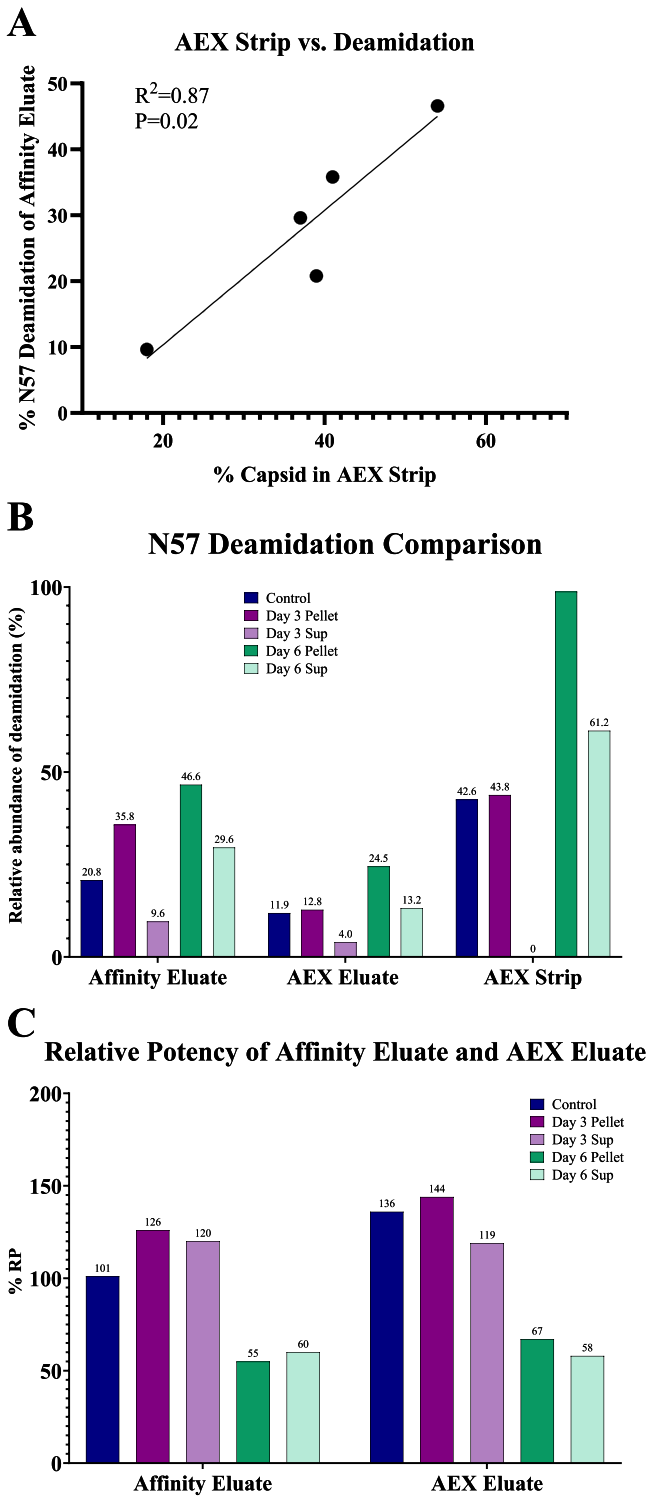

FIGURE 4 | Impact of affinity eluate N57 deamidation on AEX mass balance and enrichment. (A) A correlation analysis was performed between N57 deamidation levels of the affinity eluate and the corresponding capsid percentage of the AEX Strip. Affinity eluate N57 deamidation was measured by LC–MS. The capsid percentage of AEX Strip was calculated by dividing the total capsid count in the AEX Strip by the total capsid counts loaded onto the AEX column. This percentage measures the proportion of capsid with more surface charge. The correlation between AF product deamidation and percentage of AAV in AEX strip is statistically significant ($p = 0.02$). An R^2 value of 0.87 suggests the correlation is linear, meaning N57 deamidation may lead to increased negative charge of AAV capsid. (B) Deamidation level comparison between the affinity eluate, AEX eluate, and AEX strip. The AEX strip sample from Day 3 supernatant was not tested for LC–MS testing because the AAV concentration was below the detection limit. Data suggest that AAV in the cell pellet had a higher degree of deamidation compared to the supernatant samples, regardless of production time. However, the level of deamidation increased over time, suggesting additional surface modification occurred during the extended production. (C) Relative potency was measured for the affinity eluate and AEX eluate samples under each production condition. The control, Day 3 Supernatant and Cell Pellet samples had consistent potency within assay variability. A significant potency decline was observed when production duration was extended to 6 days.

GFP expression. Figure 4C presents the relative GFP expression levels from both affinity-purified and AEX-purified eluates under various production conditions. A notable reduction in GFP expression was observed from Day 6 versus Day 3 AAV vector particles. This decline in potency was inversely proportional to the level of deamidation at the VP1 N57 residue, confirming the critical role of VP1 during AAV cell entry and intracellular trafficking. Notably, we measured a modest increase in the GFP expression of several production conditions post-AEX purification. The hypothesis is that removing deamidated and empty capsid increased the proportion of active AAV particles. However, given the presence of other capsid heterogeneity factors, such as the charge, hydrophobicity, and additional PTMs, we could not directly correlate AAV functional expression to a single product quality attribute. Interestingly, minimal differences in potency were detected between the cell pellet and supernatant fractions from the same production duration (e.g., Day 6 Pellet vs. Day 6 Supernatant), indicating that localization does not significantly impact vector functionality.

Despite all other contributing variables in addition to deamidation, substantial deamidation at N57 consistently resulted in poor biological activity, suggesting its potential as a product quality indicator during high-throughput screening. However, an in-vitro potency assay is still required to determine the overall product functionality.

4 | Conclusions

Findings in this study indicate that production duration and localization of AAV (intracellular vs. extracellular) are key contributors to capsid heterogeneity, particularly in relation to packaging efficiency, charge profile, hydrophobicity, and PTMs such as deamidation. AAV vectors that experienced extended production duration exhibited higher levels of empty capsids and deamidation of VP1, resulting in hydrophobicity and charge profile modification. Intracellular capsids consistently showed greater deamidation and more empty capsids than their extracellular counterparts. We also established a correlation between N57 deamidation and capsid charge, which was found to influence vector behavior during AEX purification, impacting AAV functional activities. Based on the study results, we recommend minimizing production duration when sufficient productivity is reached to limit capsid heterogeneity. When

TABLE 2 | Assessment of purity via CE-SDS of each AEX eluate purified (A) and each AEX strip purified (B).

Arm	%Purity	VP1%	VP2%	VP3%	VP ratios		
(A) CE-SDS results of AEX eluate of each production condition							
Day 3 Pellet	99.1	8.3	9.2	81.7	1.0	1.1	9.8
Day 3 Sup	99.6	8.3	9.3	82.0	1.0	1.1	9.9
Day 6 Pellet	99.3	7.1	8.1	84.1	1.0	1.1	11.8
Day 6 Sup	100.0	8.9	10.5	80.6	1.0	1.2	9.1
(B) CE-SDS results of AEX strip of each production condition							
Day 3 Pellet	100.0	9.1	9.3	81.6	1.0	1.0	9.0
Day 3 Sup	97.7	7.5	8.5	81.2	1.0	1.1	10.8
Day 6 Pellet	99.3	8.1	9.1	81.7	1.0	1.1	10.1
Day 6 Sup	99.7	8.4	9.8	81.5	1.0	1.2	9.7

production duration is fixed, a robust AEX purification step should be considered to remove empty and deamidated capsids and further improve product quality consistency.

Author Contributions

Xiaotong Fu, Alex Meola, Sarah Laughlin, Thomas Thiers, Yongseok Kim, and Qi Zhang drafted the manuscript. Alex Meola, Thomas Thiers, Eli Wiberg, Luke Mustich, Sarah Laughlin, Eugenia Fandunyan, Jin Yin, Michael Mercaldi, and Richa Jaiswal designed the experiments. Alex Meola, Thomas Thiers, Eli Wiberg, Luke Mustich, Sarah Laughlin, Matt Perez, Ben Rogers, Evan DaSilva, David Rouleau, Rudenc Lushi, Rob Horton, and Yongseok Kim executed experiments and analyzed data. Ify Iwuchukwu and James McGivney reviewed the manuscript.

Acknowledgments

The authors thank Diane Golebiowski, Laura Van Lieshout, and Jeff Gagnon for supporting the conceptualization and execution of this project. They acknowledge Oxford Biomedica (US) LLC for funding this project.

Conflicts of Interest

The authors declare no conflicts of interest.

Data Availability Statement

The data that support the findings of this study are available from the corresponding author upon reasonable request.

References

Ayuso, E., F. Mingozzi, and F. Bosch. 2010. "Production, Purification and Characterization of Adeno-Associated Vectors." *Current Gene Therapy* 10, no. 6: 423–436. https://doi.org/10.2174/156652310793797685.

Bulcha, J. T., Y. Wang, H. Ma, P. Tai, and G. Gao. 2021. "Viral Vector Platforms Within the Gene Therapy Landscape." *Signal Transduction and Targeted Therapy* 6, no. 1: 53. https://doi.org/10.1038/s41392-021-00487-6.

Burnham, B., S. Nass, E. Kong, et al. 2015. "Analytical Ultracentrifugation as an Approach to Characterize Recombinant Adeno-Associated Viral Vectors." *Human Gene Therapy Methods* 26, no. 6: 228–242. https://doi.org/10.1089/hgtb.2015.048.

Clément, N., and J. C. Grieger. 2016. "Manufacturing of Recombinant Adeno-Associated Viral Vectors for Clinical Trials." *Molecular Therapy – Methods & Clinical Development* 3: 16002. https://doi.org/10.1038/mtm.2016.2.

Dickerson, R., C. Argento, J. Pieracci, and M. Bakhshayeshi. 2021. "Separating Empty and Full Recombinant Adeno-Associated Virus Particles Using Isocratic Anion Exchange Chromatography." *Biotechnology Journal* 16, no. 1: 202000015. https://doi.org/10.1002/biot.202000015.

DiMattia, M. A., H.-J. Nam, K. Van Vliet, et al. 2012. "Structural Insight Into the Unique Properties of Adeno-Associated Virus Serotype 9." *Journal of Virology* 86, no. 12: 6947–6958. https://doi.org/10.1128/jvi.07232-11.

Fu, X., W.-C. Chen, C. Argento, et al. 2019. "Analytical Strategies for Quantification of Adeno-Associated Virus Empty Capsids to Support Process Development." *Human Gene Therapy Methods* 30, no. 4: 144–152. https://doi.org/10.1089/hgtb.2019.088.

Fuentes, C., J. Staudhammer, J. F. Wright, et al. n.d. "Dark Horse Consulting Group Beyond Empty and Full: Understanding Heterogeneity in RAAV Products and Impurities."

Giles, A., M. Lock, S.-J. Chen, et al. 2023. "Significant Differences in Capsid Properties and Potency Between Adeno-Associated Virus Vectors Produced in Sf9 and HEK293 Cells." *Human Gene Therapy* 34, no. 19–20: 1003–1021. https://doi.org/10.1089/hum.2022.116.

Giles, A. R., J. J. Sims, K. B. Turner, et al. 2018. "Deamidation of Amino Acids on the Surface of Adeno-Associated Virus Capsids Leads to Charge Heterogeneity and Altered Vector Function." *Molecular Therapy* 26, no. 12: 2848–2862. https://doi.org/10.1016/j.ymthe.2018.09.013.

Grieger, J. C., S. Snowdy, and R. J. Samulski. 2006. "Separate Basic Region Motifs Within the Adeno-Associated Virus Capsid Proteins Are Essential for Infectivity and Assembly." *Journal of Virology* 80, no. 11: 5199–5210. https://doi.org/10.1128/jvi.02723-05.

Kronenberg, S., B. Böttcher, C. W. von der Lieth, S. Bleker, and A. Kleinschmidt. 2005. "A Conformational Change in the Adeno-Associated Virus Type 2 Capsid Leads to the Exposure of Hidden VP1 N Termini." *Journal of Virology* 79, no. 9: 5296–5303. https://doi.org/10.1128/jvi.79.9.5296-5303.2005.

MacLean, B., D. M. Tomazela, N. Shulman, et al. 2010. "Skyline: An Open Source Document Editor for Creating and Analyzing Targeted Proteomics Experiments." *Bioinformatics* 26, no. 7: 966–968. https://doi.org/10.1093/bioinformatics/btq054.

McColl-Carboni, A., S. Dollive, S. Laughlin, et al. 2024. "Analytical Characterization of Full, Intermediate, and Empty AAV Capsids." *Gene Therapy* 31, no. 5–6: 285–294. https://doi.org/10.1038/s41434-024-00444-2.

Penzes, J. J., P. Chipman, N. Bhattacharya, et al. 2021. "Adeno-Associated Virus 9 Structural Rearrangements Induced by Endosomal

Trafficking pH and Glycan Attachment." *Journal of Virology* 95, no. 19: e00843-2. https://doi.org/10.1128/jvi.00843-21.

Popa-Wagner, R., M. Porwal, M. Kann, et al. 2012. "Impact of VP1-Specific Protein Sequence Motifs on Adeno-Associated Virus Type 2 Intracellular Trafficking and Nuclear Entry." *Journal of Virology* 86, no. 17: 9163–9174. https://doi.org/10.1128/jvi.00282-12.

Sonntag, F., S. Bleker, B. Leuchs, R. Fischer, and A. Kleinschmidt. 2006. "Adeno-Associated Virus Type 2 Capsids With Externalized VP1/VP2 Trafficking Domains Are Generated Prior to Passage Through the Cytoplasm and Are Maintained Until Uncoating Occurs in the Nucleus." *Journal of Virology* 80, no. 22: 11040–11054. https://doi.org/10.1128/jvi.01056-06.

van Lieshout, L. P., M. Rubin, K. Costa-Grant, et al. 2023. "A Novel Dual-Plasmid Platform Provides Scalable Transfection Yielding Improved Productivity and Packaging Across Multiple AAV Serotypes and Genomes." *Molecular Therapy – Methods & Clinical Development* 29: 426–436. https://doi.org/10.1016/j.omtm.2023.05.004.

Venkatakrishnan, B., J. Yarbrough, J. Domsic, et al. 2013. "Structure and Dynamics of Adeno-Associated Virus Serotype 1 VP1-Unique N-Terminal Domain and Its Role in Capsid Trafficking." *Journal of Virology* 87, no. 9: 4974–4984. https://doi.org/10.1128/jvi.02524-12.

Wörner, T. P., A. Bennett, S. Habka, et al. 2021. "Adeno-Associated Virus Capsid Assembly Is Divergent and Stochastic." *Nature Communications* 12, no. 1: 1642. https://doi.org/10.1038/s41467-021-21935-5.

Wright, J. F. 2014. "AAV Empty Capsids: For Better or for Worse?" *Molecular Therapy* 22, no. 1: 1–2. https://doi.org/10.1038/mt.2013.268.

Wu, J., B. E. Draper, M. F. Jarrold, et al. 2025. "Insights Into Adeno-Associated Virus Capsid Charge Heterogeneity." *Analytical Chemistry* 97: 17132–17140. https://doi.org/10.1021/acs.analchem.5c03104.

Zhou, Y., and Y. Wang. 2023. "Direct Deamidation Analysis of Intact Adeno-Associated Virus Serotype 9 Capsid Proteins Using Reversed-Phase Liquid Chromatography." *Analytical Biochemistry* 668: 115099. https://doi.org/10.1016/j.ab.2023.115099.

Supporting Information

Additional supporting information can be found online in the Supporting Information section.

Supporting File: bit70219-sup-0001-Supplemental_info_revision_1.docx.